Improved Cycle Performance of Li-CO_2 Batteries with Nickel Manganite Supported Carbon Nanotube $NiMn_2O_4$ @CNT Cathode

Journal of The Electrochemical Society, 2023 **170** 090513
1945-7111/2023/170(9)/090513/6/$40.00 © 2023 The Electrochemical Society ("ECS"). Published on behalf of ECS by IOP Publishing Limited

Improved Cycle Performance of Li-CO_2 Batteries with Nickel Manganite Supported Carbon Nanotube $NiMn_2O_4$ @CNT Cathode

Jianda Wang,[1] Matthew Powell,[1] Ryan Alcala,[1] Christopher Fetrow,[1] Xiao-Dong Zhou,[2,z] and Shuya Wei[1,z]

[1]*Department of Chemical and Biological Engineering, University of New Mexico, Albuquerque, New Mexico 87131, United States of America*
[2]*Department of Chemical Engineering, Institute for Materials Research and Innovations, University of Louisiana at Lafayette, Louisiana 70504, United States of America*

Rechargeable Li-CO_2 batteries have emerged as promising candidates for next generation batteries due to their low cost, high theoretical capacity, and ability to capture the greenhouse gas CO_2. However, these batteries still face challenges such as slow reaction kinetic and short cycle performance due to the accumulation of discharge products. To address this issue, it is necessary to design and develop high efficiency electrocatalysts that can improve CO_2 reduction reaction. In this study, we report the use of $NiMn_2O_4$ electrocatalysts combined with multiwall carbon nanotubes as a cathode material in the Li-CO_2 batteries. This combination proved effective in decomposing discharge products and enhancing cycle performance. The battery shows stable discharge–charge cycles for at least 30 cycles with a high limited capacity of 1000 mAh g^{-1} at current density of 100 mA g^{-1}. Furthermore, the battery with the $NiMn_2O_4$@CNT catalyst exhibits a reversible discharge capacity of 2636 mAh g^{-1}. To gain a better understanding of the reaction mechanism of Li-CO_2 batteries, spectroscopies and microscopies were employed to identify the chemical composition of the discharge products. This work paves a pathway to increase cycle performance in metal-CO_2 batteries, which could have significant implications for energy storage and the reduction of greenhouse gas emissions.
 [DOI: 10.1149/1945-7111/acf623]

Manuscript submitted May 21, 2023; revised manuscript received July 18, 2023. Published September 12, 2023.

Non-renewable fossil fuels continue to be a significant source of energy. However, the combustion of carbon dioxide (CO_2) from these fuels is a primary contributor to the the greenhouse effect.[1] Moreover, with the increasing demand for energy, finding solutions to address this challenge has become more pressing.[2–4] Energy storage devices that can alleviate energy shortages and capture the greenhouse gas CO_2 are urgently needed.[5,6] Li-CO_2 batteries have become a promising solution for next-generation energy storage devices due to the high specific energy and ability to recycle CO_2.[7–9] The concept of Li-CO_2 batteries was first proposed by Archer's group, who were investigating how CO_2 contamination affects Li-O_2 batteries.[10] Nowadays, Li-CO_2 batteries are considered a viable option for large scale energy storage devices due to the utilization of CO_2 as the active cathode and still have a high energy capacity, which is approximately 10 times that of the currently commercialized Li-ion batteries.[11,12] However, according to equation: $4Li + 3CO_2 \leftrightarrow 2Li_2CO_3 + C$, the main discharge product Li_2CO_3 needed high voltage to decompose, which causes low energy efficiency, poor cycle performance and higher safety risk to Li-CO_2 batteries.[13,14] Therefore, it is important to find a facile way to effectively decompose discharge product to decrease overpotential and enhance cycle performance.

Many groups designed and developed various electrocatalysts to assist the decomposition of discharge product, including carbon-based,[15–17] noble metal-based,[18,19] transition metal-based[20–22] and organic polymer-based electrocatalysts.[23–25] Among these electrocatalysts, carbon-based electrocatalysts, such as carbon nanotubes (CNTs), can provide high surface area for electrolyte and CO_2 diffusion and avoid the accumulation of the discharge product. Low cost and high electrical conductivity are also advantages of carbon-based electrocatalysts.[15] Besides, transition metal-based electrocatalysts are recognized as a promising candidate for enhancing sluggish reaction kinetic and improving cycle performance of Li-CO_2 batteries. Notably, complex transition metal oxides providing more redox mediating sites have shown better catalytic performance than single transition metal oxides. For examples, Liu's group reported complex transition metal oxides $ZnCo_2O_4$ nanorods as electrocatalysts for Li-CO_2 batteries.[26] Li-CO_2 batteries using $ZnCo_2O_4$@CNT can achieve higher discharging capacity and better cycle performance than Co_3O_4@CNT cathode at the same current density. In addition, Deng et al. synthesized MnO_x-CeO_2@Polypyrrole (MnO_x-CeO_2@ppy) structural cathode to promote cycle performance and discharging ability for Li-CO_2 batteries, the results show that Li-CO_2 batteries with MnO_x-CeO_2@ppy can achieve the best cycling property and longest discharging time compared with other types of cathode catalysts (MnO_x @ppy and CeO_2@ppy), which shows enhanced electron deliver capacity for MnO_x-CeO_2.[27]

In this work, we synthesized $NiMn_2O_4$ electrocatalysts using sol-gel method on a carbon paper substrate to study the catalytic performance of $NiMn_2O_4$@CNT cathode catalysts in rechargeable Li-CO_2 batteries. The results show that Li-CO_2 batteries with a $NiMn_2O_4$@CNT cathode composite achieve a reversible discharge capacity of 2636 mAh g^{-1}. The coulombic efficiency reached 100% for charging the batteries over 30 cycles at a high limited capacity of 1000 mAh g^{-1} (current density: 100 mA g^{-1}). This improved cycle performance and superior catalytic performance of the cathode are attributed to the excellent catalytic ability of $NiMn_2O_4$ electrocatalysts and synergistic effect with CNTs.

Experimental

Preparation of $NiMn_2O_4$.—The sol-gel method was performed by dissolving polyvinylpyrrolidone (PVP) into 100 ml of DI water under stirring for 1 h. Then, 5 g PVP, 3.1 g nickel nitrate hexahydrate and 5.1 g manganese nitrate tetrahydrate are added to DI water at the same time to gain a homogeneous mixture. The sol of the compounds $NiMn_2O_4$ was continuously stirred with a magnetic stirrer. Then, the solution was stirred for 1 h and placed in an oven to dry at 110 °C for removing residual water. The resulting gel was crushed and calcined and followed by heating at 750 °C to obtain a crystalline powder. NiO and Mn_2O_3 electrocatalysts are synthesized by similar methods. For example, to synthesize NiO, manganese nitrate tetrahydrate is removed from the previous recipe and the precursor is calcined at 750 °C.

Instrumentation and characterization measurement.—Powder X-ray diffraction (XRD) patterns of the cathodes were recorded with Rigaku SmartLab X-ray diffractometer. The morphologies of the pristine, discharged, and recharged $NiMn_2O_4$@CNT cathode were collected by scanning electron microscopy (SEM) Tescan Vega 3. Chemical compositions of the electrodes were recorded by X-ray photoelectron spectrometry (XPS) Kratos AXIS ULTRA X-ray

[z]E-mail: xiao-dong.zhou@louisiana.edu; swei@unm.edu

Photoelectron Spectrometer. Electrochemical impedance spectroscopy (EIS) measurements of $NiMn_2O_4$@CNT cathode were examined by biologic electrochemical potentiostat VSP3 at 5 mV AC amplitude and frequencies from 200 kHz to 100mHz. Fourier-transform infrared spectroscopy (FT-IR) measurement was performed by Nicolet 6700 FT-IR spectrometer.

Cathodes preparation.—Synthesized $NiMn_2O_4$ electrocatalysts and multiwalled CNTs were dispersed in poly(vinylidene fluoride) (PVDF) and mixed with NMP solvent. The weight ratio for $NiMn_2O_4$:CNT:PVDF is 47:47:6. The obtained mixture was ball-milled for 1.5 h to prepare a homogeneous slurry. Then, the homogeneous slurry was drop-cast onto carbon paper at 20 μm thickness and was vacuum heated at 50 °C overnight to remove NMP solvent. The final products were used as the cathode for Li-CO_2 batteries. For the preparation of the NiO@CNT and Mn_2O_3@CNT slurry, replacing $NiMn_2O_4$ with NiO (Mn_2O_3) and using same steps can prepare NiO@CNT and Mn_2O_3@CNT, respectively. For preparation of pure CNT cathode, mixed CNT slurry was prepared by using CNTs and poly(vinylidene fluoride) in NMP solvent with weight ratio of 94:6. The cathode preparation method followed the similar process. All cathodes for electrochemical tests were similar amount of catalyst loading (~1 mg) and Ar-filled glovebox was used to store all synthesized electrodes.

Swagelok battery assembly.—Assembling Li-CO_2 batteries with Swagelok cell-type were in an Ar-filled glovebox by anode: Li foil, cathode: synthesized $NiMn_2O_4$@CNT on carbon paper, electrolyte: 1 M lithium bis(trifluoromethanesulfonyl)imidedissolved (LiTFSi) in tetraethylene glycol dimethyl ether (TEGDME) solvent, as well as separator: glass fibers. CO_2 injection for Swagelok cell was through mass flow controller that connected to a CO_2 gas cylinder at a flow rate of 8 ml s^{-1}. This process lasts for an hour to ensure getting enough carbon dioxide in the cell, and Swagelok cell was sealed after getting enough CO_2 to avoid air entry.

Results and Discussion

The crystallographic structure of prepared electrocatalysts $NiMn_2O_4$ were identified by the XRD characterization measurement as shown in Fig. 1, XRD pattern shown 2 θ value from 10° to 75° to record the prominent peaks of spinel $NiMn_2O_4$. Peaks at 2 θ value of 18.3°, 30.0°, 35.5°, 37.0°, 42.9°, 53.2°, 56.8° and 62.5° were respectively indexed to the (111), (220), (311), (222), (400), (422), (511) and (440) planes of $NiMn_2O_4$ spinel.[28] XRD pattern of Mn_2O_3 and NiO are exhibited in Fig. S1. According to the XRD pattern, NiO can be confirmed by peaks at 37.1°, 43.1°, 62.9°, 75.2°, and 79.3°, which can respectively be indexed to (111), (200), (220), (311), and (222) phase. Mn_2O_3 can be confirmed by peaks at 23.1°, 32.9°, 38.1°, 45.1°, 49.4°, and 65.9°. These peaks can be indexed to (211), (222), (400), (332), (134), (440) and (622) phase.[29,30]

XPS technology was adopted to analyze the oxidation state and elemental composition of $NiMn_2O_4$ electrocatalyst (Fig. 2). Full survey spectra of $NiMn_2O_4$ are shown in Fig. 2a, which confirms the existence of Ni, Mn and O elements. To further investigate oxidation state for these elements, high resolution spectrum of Mn 2p, Ni 2p and O 1s clearly exhibit Ni, Mn, and O elements. Figure 2b shows the high-resolution spectrum of Ni 2p (Ni $2p_{1/2}$ and Ni $2p_{3/2}$). Ni $2p_{3/2}$ could be identified according to two representative peaks at 854.5 and 856.3 eV, and two peaks located at 871.5 and 873.3 eV corresponds to the Ni $2p_{1/2}$.[31] Two peaks at 860.9 and 879.3 eV could be attributed to satellite (Sat.) peaks of the Ni $2p_{1/2}$ and Ni $2p_{3/2}$, respectively, which match with previous reported results.[32] The coexistence of Ni^{2+} (peaks at 856.3 and 873.3 eV) and Ni^{3+} (peaks at 854.5 and 871.5 eV) in $NiMn_2O_4$ is confirmed by these results. Figure 2c shows the high-resolution spectrum of Mn 2p (Mn $2p_{1/2}$ and Mn $2p_{3/2}$). Four peaks shown in Fig. 2c come from deconvolved process of two spin–orbit peaks in Mn spectrum.[33] Two deconvolved peaks located at 641.2 and 643.0 eV correspond to Mn $2p_{3/2}$. Two deconvolved peaks observed at 654.5 and 652.5 eV could be attributed to Mn $2p_{1/2}$.[34] The set of peaks at 641.2 and 652.5 eV could correspond to the existence of Mn^{2+}, and another set of peaks at 642.5 and 654.0 eV correspond to the correlative peaks of Mn^{3+}. These results revealed coexistence of Mn^{2+}/Mn^{3+} in $NiMn_2O_4$. High resolution spectrum O1 s is shown in Fig. 2d. The prominent peak for O 1 s at 529.4 eV could be attributed to lattice oxygen or metal oxygen bonds (M-O-M), the resolved peaks at 530.8 eV is indexed to metal-O–H from metal surface hydroxyl groups, and existence of defect sites with a low oxygen coordination could be confirmed by peaks at 532.2 eV, which shown a typical feature of materials with small particles.[35]

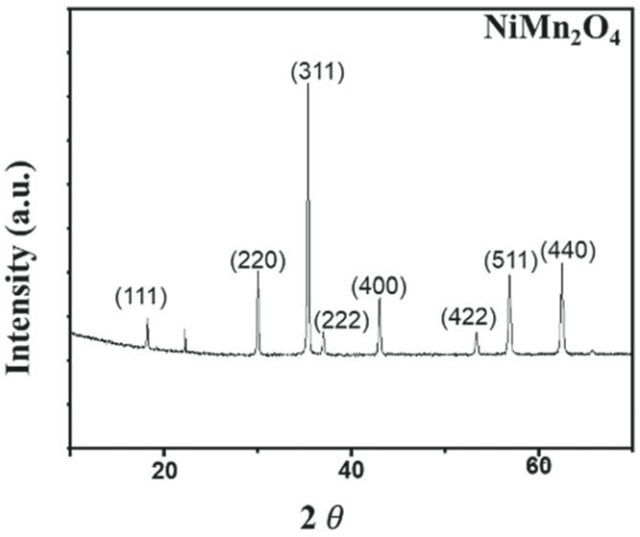

Figure 1. X-ray diffraction pattern of different types of electrocatalysts: $NiMn_2O_4$, NiO and Mn_2O_3.

Galvanostatic charge/discharge tests were performance to study the electrocatalytic activity of $NiMn_2O_4$ towards the decomposition of discharge product, electrochemical performance of Li-CO_2 batteries with different catalytic cathodes were tested as shown in Fig. 3. Figure 3a shows the discharge-charge curves of Li-CO_2 batteries with the pure CNT cathodes with a high cut-off capacity of 1000 mA h g^{-1} (current density:100 mA g^{-1}), and Fig. 3b shows the cycle performance of Li-CO_2 batteries with $NiMn_2O_4$@CNT cathode with same cut-off capacity and same current density. The results clearly show that without the addition of the $NiMn_2O_4$ electrocatalyst, Li-CO_2 batteries can only achieve 5 cycles, and then the overpotential rapidly rises beyond the set range. By comparison, the cycle performance of Li-CO_2 batteries with $NiMn_2O_4$@CNT cathode is greatly improved, which runs exceeds 30 cycles. This result shows that the catalyst has a better catalytic ability to decompose discharge products of Li-CO_2 batteries. Cycle performance of Na-CO_2 batteries with $NiMn_2O_4$@CNT and CNT cathode were also tested to further study catalytic performance of $NiMn_2O_4$@CNT electrode (Fig. S1). The results show $NiMn_2O_4$@CNT cathode also can effectively enhance cycling profile for Na-CO_2 batteries. Figure 3c directly exhibits the relationship between cycle numbers and corresponding end terminal voltages. The results reveal that Li-CO_2 batteries with $NiMn_2O_4$@CNT cathode can maintain a reasonable discharging and charging plateau of 2.5 V and 4.5 V respectively for a longer time, which also indicates the stability of $NiMn_2O_4$@CNT cathode. Li-CO_2 batteries with different types of cathodes ($NiMn_2O_4$@CNT, Mn_2O_3@CNT, NiO@CNT and CNTs) were tested to investigate discharging ability in a range of 1.5–3.5 V (Fig. 3d). Li-CO_2 batteries with $NiMn_2O_4$@CNT cathode own the highest discharging capacity (2636 mAh g^{-1}), which is better than the case of Mn_2O_3@CNT (1829 mAh g^{-1}) and NiO@CNT (1818 mAh g^{-1}). The results show complex transition metal oxide ($NiMn_2O_4$) has better catalytic performance for CO_2 reduction than single transition metal

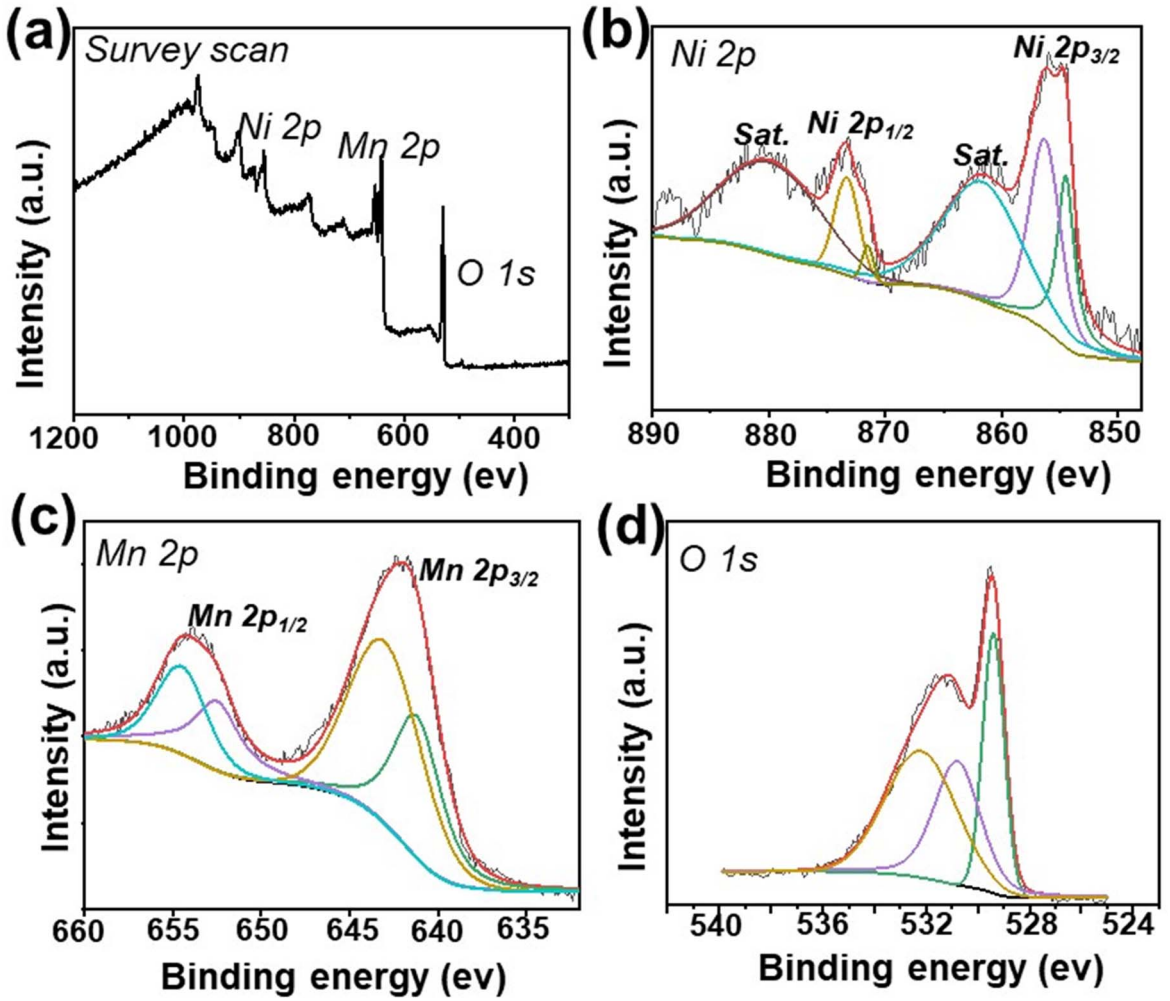

Figure 2. (a) X-ray photoelectron spectroscopy (XPS) survey scan spectra of $NiMn_2O_4$ electrocatalysts. (b) Ni 2p spectrum. (c) Mn 2p spectrum. (d) O 1s spectrum. These black and red curves correspond to the experimental and fitted curves of the spectra of Ni 2p, Mn 2p and O 1s.

oxide (Mn_2O_3 and NiO). Li-CO_2 batteries with pure CNT cathode have the lowest discharging ability (1257 mAh g^{-1}). The improved electrochemical performance of $NiMn_2O_4$@CNT cathode was attributed to synergistic effect of $NiMn_2O_4$ and CNT, as well as catalytic ability of $NiMn_2O_4$ to promote CO_2 diffusion during discharging process.

Cyclic voltammetry (CV) tests were performed with a slow scan rate (0.1 mV s^{-1}) to analyze electrochemical behavior for Li-CO_2 batteries with different electrocatalysts ($NiMn_2O_4$, Mn_2O_3, NiO and pure CNT) as shown in Fig. S3. It can be noticed that Li-CO_2 batteries with $NiMn_2O_4$@CNT cathode have a higher cathodic peak (~0.1 mA at 4.5 V) compared with other electrocatalysts, which reveals a stronger CO_2 reduction reaction during cathodic scanning. In this case, the starting point of cathodic peak for $NiMn_2O_4$@CNT cathode catalysts is at ~2.5 V in range of 2–4.5 V, it reveals the decomposition of the discharge product Li_2CO_3.

Ex-situ SEM characterization measurement was adopted on the $NiMn_2O_4$@CNT cathode to investigate discharge products and to evaluate electrochemical charging/discharging process of the Li-CO_2 batteries. Figure 4 shows the morphology change of $NiMn_2O_4$@CNT cathode of 1st cycle's pristine, discharged, and recharged stages with a limited capacity of 1000 mAh g^{-1} at current density 100 mA g^{-1}. As shown in Fig. 4a, CNTs provide a large surface area to assist electrolyte/CO_2 diffusion and $NiMn_2O_4$ electrocatalysts on the surface of CNTs to suffer catalytic sites for decomposition of discharge product of Li-CO_2 batteries. By comparing Figs. 4b with 4c, morphology of recharged electrode has been changed due to accumulation of discharge product, and the morphology of recharged electrode is closer to pristine electrode, which indicates that the $NiMn_2O_4$ electrocatalyst can effectively degrade discharge product. In addition, the structure of $NiMn_2O_4$ electrocatalysts does not evolve in all types of cathodes, which reveals that $NiMn_2O_4$ electrocatalysts are stable over cycling.

To further understand the role of $NiMn_2O_4$@CNT for Li-CO_2 batteries to improve cycling properties, ex situ XPS were performed to further study the reaction mechanism of Li-CO_2 batteries and to identify chemical composition of discharge product. XPS characterization measurement can effectively identify the change of surface properties for discharged and recharged $NiMn_2O_4$@CNT cathode. The comparison of C 1s spectrum of discharged and recharged $NiMn_2O_4$@CNT cathode shown in Figs. 5a and 5b, Fig. 5a displays representative peak at 289.5 eV to confirm the formation of discharge product Li_2CO_3, and the peak related to Li_2CO_3 almost disappears after recharging process (Fig. 5b).[36] Decreased C-C peak (284.1 eV) intensity for discharged cathode is caused by coverage of discharge product.[37] For Li 1s spectrum, peak of Li_2CO_3 (55.5 eV) can also be observed (Fig. 5c), and this peak becomes weak after recharging process shown in Fig. 5d.[38] Therefore, these results not only can identify the chemical composition but also show the ability of $NiMn_2O_4$ electrocatalysts to decompose Li_2CO_3. In addition, the change of spectrum of Ni 2p and Mn 2p can show surface properties for $NiMn_2O_4$@CNT cathode influenced by discharging and charging process. As shown in Fig. S4, spectrums for Ni 2p and Mn 2p for these two stages have obvious change compared to pristine stage of

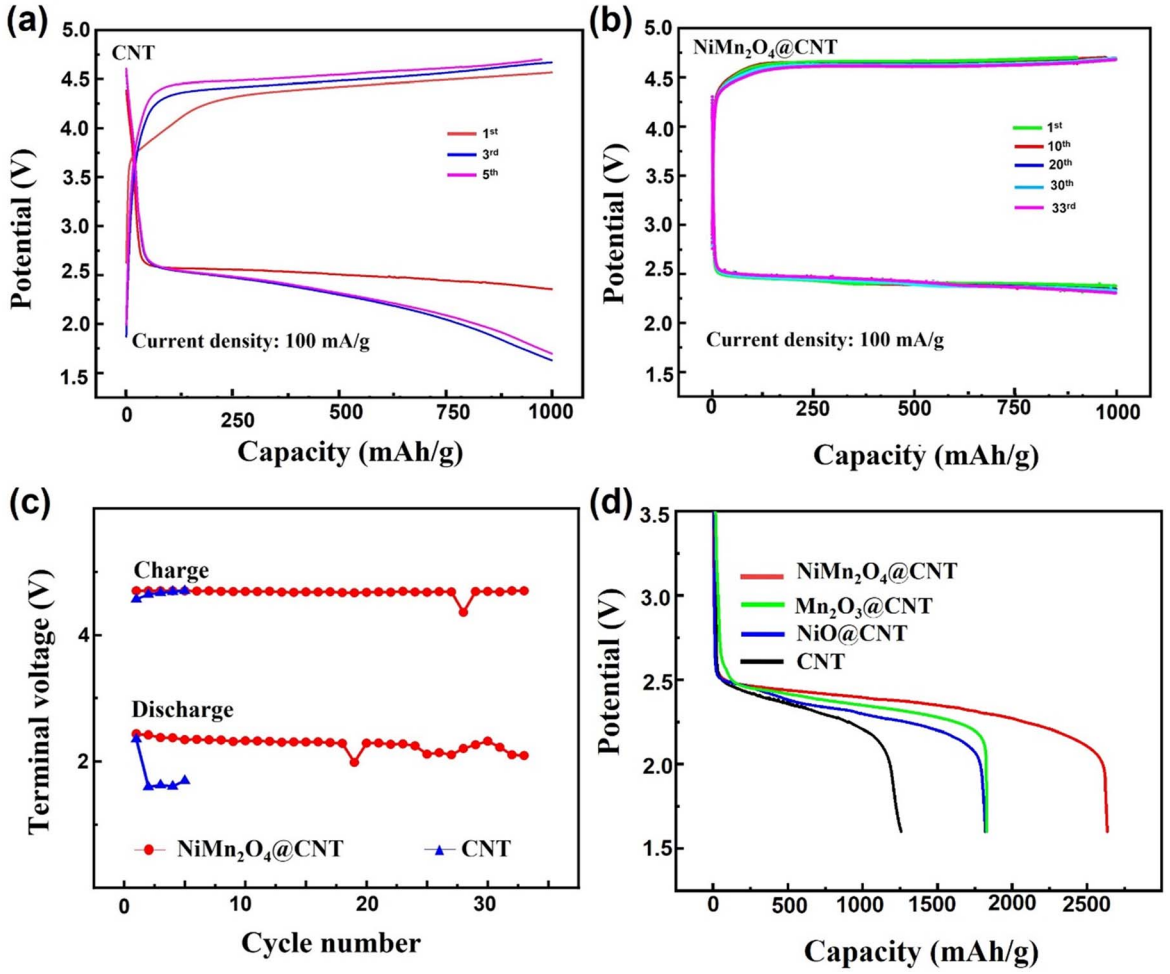

Figure 3. (a) Cycle performance of Li-CO_2 batteries with pure CNT cathode at current density of 100 mA g^{-1}; (b) Cycle performance of Li-CO_2 batteries with $NiMn_2O_4$@CNT cathode at current density of 100 mA g^{-1}; (c) Discharging ability of Li-CO_2 batteries with different types of cathode ($NiMn_2O_4$@CNT, Mn_2O_3@CNT, NiO@CNT and pure CNT) at current density of 100 mA g^{-1}; (d) Charge/discharge cycling performance and end terminal voltages for $NiMn_2O_4$@CNT and pure CNT cathode at current density of 100 mA g^{-1} in Li-CO_2 batteries.

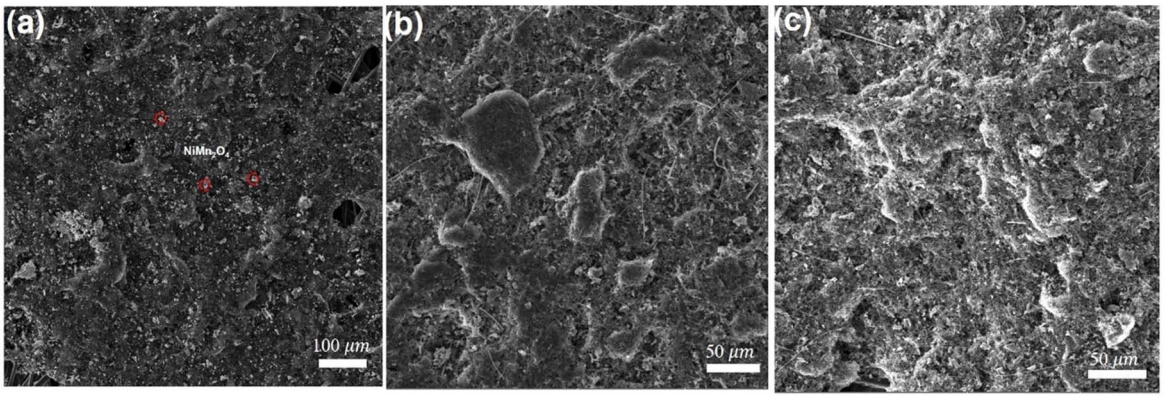

Figure 4. SEM images of $NiMn_2O_4$@CNT cathode of different stages with a limited capacity of 1000 mAh g^{-1} and current density of 100 mA h^{-1}: (a) pristine cathode, (b) discharged cathode and (c) recharged cathode.

$NiMn_2O_4$, it can be noticed that peaks for Ni $2p_{1/2}$/Ni $2p_{3/2}$ and Mn $2p_{1/2}$/Mn $2p_{3/2}$ became weaken after the discharge process (Figs. S4a and S4c). The reason could contribute to coverage of discharged products on the cathodic surface. After the recharging process, the peaks are still different from original stage in $NiMn_2O_4$ (Figs. S4b and S4d), we believe that it comes from ratio change of Ni^{2+}/Ni^{3+} and Mn^{2+}/Mn^{3+}, and these changes could promote the decomposition of discharged product.

FT-IR (Fig. 6 and Ex-situ XRD (Fig. S5) were also adopted to further formation of discharged product and role of electrocatalysts. According to results of FT-IR, spectrum of discharged $NiMn_2O_4$@CNT cathode has a peak at ~1510 cm^{-1} to identify the formation Li_2CO_3, and this peak almost disappeared after recharging process.[39] This result is consistent with XPS measurement. In addition, XRD pattern shows additional peaks in discharged $NiMn_2O_4$@CNT cathode at 23.7° and 36.9° are indexed to (200) and (311) planes of Li_2CO_3.

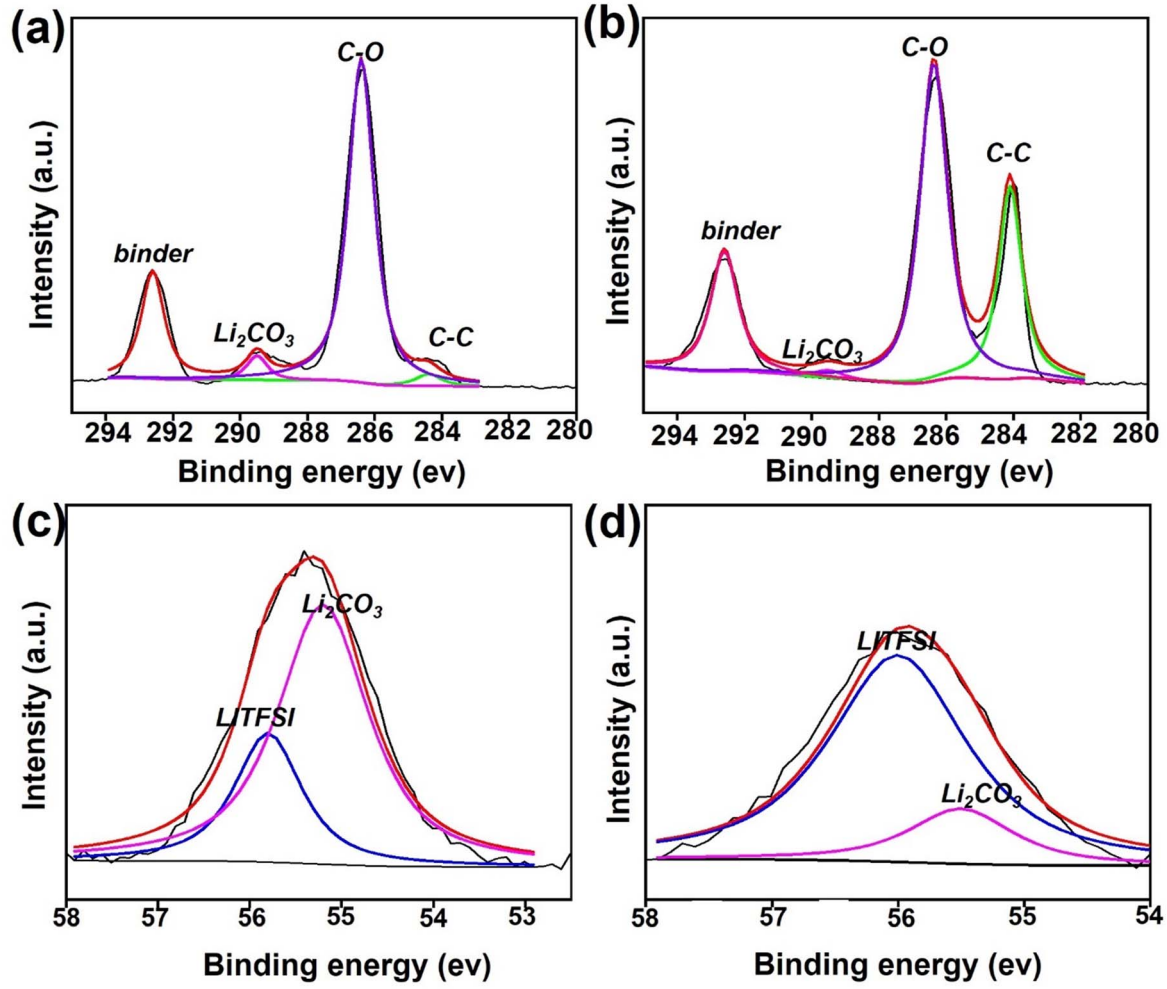

Figure 5. C 1s high-resolution X-ray photoelectron spectra of (a) discharged and (b) recharged $NiMn_2O_4$@CNT cathode (limited capacity: 1000 mAh g^{-1} and current density: 100 mA h^{-1}); Li 1 s high-resolution X-ray photoelectron spectra of (c) discharged and (d) recharged $NiMn_2O_4$@CNT cathode (limited capacity: 1000 mAh g^{-1} and current density: 100 mA h^{-1}).

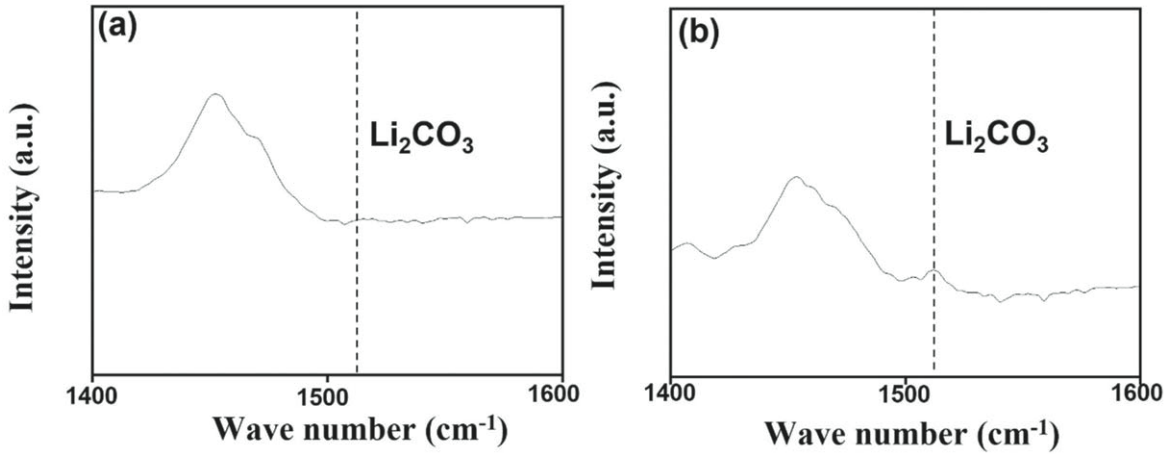

Figure 6. Ex-situ Fourier-transform infrared spectroscopy (FT-iR) measurement for different stage of $NiMn_2O_4$@CNT cathode: (a) recharged $NiMn_2O_4$@CNT cathode; (b) discharged $NiMn_2O_4$@CNT cathode.

Electrochemical impedance spectroscopy (EIS) was performed to compare the impedance patterns of Li-CO_2 batteries using $NiMn_2O_4$@CNT for different stages (pristine, fully discharged and fully recharged stage) shown in Fig. 7. Charge-transfer resistance (R_{ct}) of redox reactions happening at the electrodes is related to diameter of the semicircles. After the full discharge process, the diameter of the semicircle is significantly larger compared with pristine stage, which means an increasement of R_{ct}, and the semicircle diameter fully recharged Li-CO_2 batteries becomes smaller. The information of different resistances of impedance

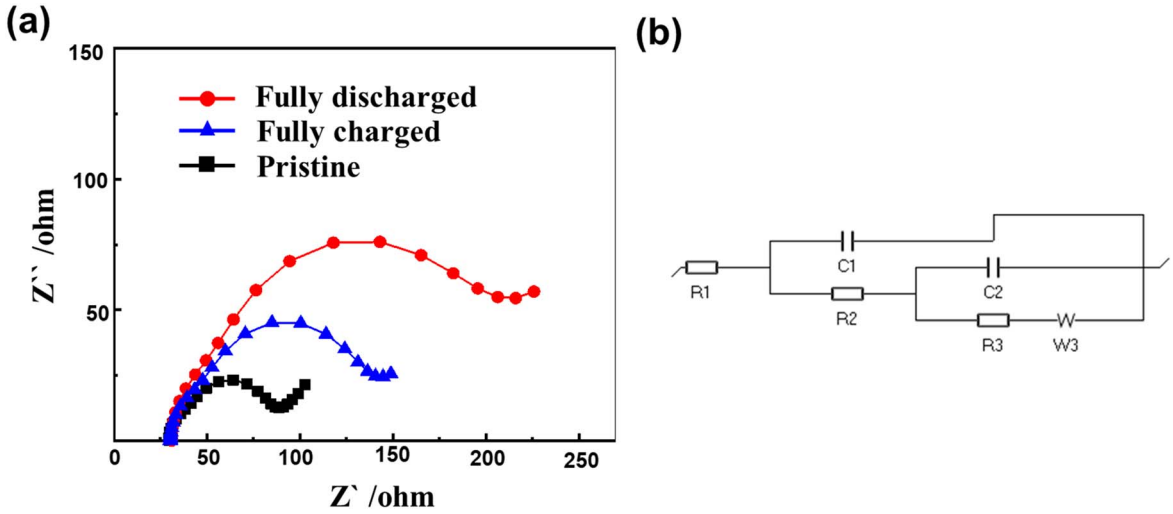

Figure 7. (a) Impedance changes of Li-CO_2 batteries with cathode material $NiMn_2O_4$@CNT for different stages: pristine, fully discharged and fully charged. (b) impedance model.

model are shown in Table S1, the results clearly show that resistance R1 R2 and R3 increase after the discharging process and decrease after the recharging process, which is consistent with formation and decomposition process for discharged product.

Conclusions

Li-CO_2 batteries are regarded as promising candidates for next generation energy storage devices due to their low price and excellent theoretical energy capacity. Therefore, it is necessary to design and develop superior electrocatalysts to effectively decompose discharge products to enhance reaction kinetic and improve cycle performance. We reported a facile sol-gel method to synthesize $NiMn_2O_4$ electrocatalysts to achieve this goal. Li-CO_2 batteries with $NiMn_2O_4$@CNT cathode can sustain 33 cycles and discharge and charge plateau remain stable at 2.48 V and 4.55 V (limited capacity: 1000 mAh g^{-1}, current density: 100 mA g^{-1}), which is a great improvement compared with cycle performance for pure CNT cathode. Li-CO_2 batteries with this type of cathode catalyst also deliver a discharge capacity of 2636 mAh g^{-1}. Li-CO_2 batteries with Mn_2O_3@CNT, NiO@CNT and pure CNT can only achieve discharge capacity of 1829, 1818 and 1257 mAh g^{-1}. These results show $NiMn_2O_4$@CNT catalyst can high-efficiency assistant CO_2 diffusion during discharging process. In addition, we also adopted multiple characterization measurements to identify the chemical composition of discharge product and study reaction mechanism ($4Li + 3CO_2 \leftrightarrow 2Li_2CO_3 + C$) of Li-$CO_2$ batteries.

This work shows excellent catalytic performance for complex transition metal oxide $NiMn_2O_4$ combined with CNT and paves a pathway for designing new electrocatalysts for Li-CO_2 batteries. The facile sol-gel method also can provide an eco-friendly and controllable way to synthesize desired electrocatalysts for next-generation metal-CO_2 batteries. In addition, shedding light on mechanism of Li-CO_2 batteries and ability of electrocatalysts would provide a solid foundation to develop suitable electrocatalysts for next step.

Acknowledgments

This work was supported by the National Science Foundation Award Number 2119688. S.W. acknowledges the financial support from the University of New Mexico startup fund.

ORCID

Xiao-Dong Zhou https://orcid.org/0000-0001-9934-9429
Shuya Wei https://orcid.org/0000-0001-9269-1950

References

1. J. Wang, B. Marchetti, X.-D. Zhou, and S. Wei, *ACS Energy Lett.*, **8**, 1818 (2023).
2. J. Gao, L. Cheng, K. Li, Y. Wang, and Z. Wu, *J. Electrochem. Soc.*, **169**, 024513 (2022).
3. R. Küngas, *J. Electrochem. Soc.*, **167**, 044508 (2020).
4. F. Liu, J. Zhu, and J. Yuan, *J. Electrochem. Soc.*, **168**, 066505 (2021).
5. Z. Jiang et al., *Energy Environ. Sci.*, **13**, 2856 (2020).
6. J. H. Zhou et al., *Angew. Chemie - Int. Ed.*, **58**, 14197 (2019).
7. D. Gao et al., *J. Am. Chem. Soc.*, **139**, 5652 (2017).
8. W. Xiong et al., *Small*, **16**, 2003943 (2020).
9. J. Lin et al., *Adv. Mater.*, **34**, 2200559 (2022).
10. S. Xu, S. K. Das, and L. A. Archer, *RSC Adv.*, **3**, 6656 (2013).
11. Z. Guo et al., *Small*, **15**, 1803246 (2019).
12. S. Bie et al., *ACS Appl. Mater. Interfaces*, **11**, 5146 (2019).
13. X. Li et al., *Adv. Mater.*, **31**, 1903852 (2019).
14. Y. Qiao et al., *Energy Storage Mater.*, **27**, 133 (2020).
15. Y. Xiao et al., *ACS Energy Lett.*, **5**, 916 (2020).
16. F. Ye et al., *Adv. Energy Mater.*, **11**, 2101390 (2021).
17. B. Chen et al., *ACS Nano*, **15**, 9841 (2021).
18. Y. Zhai et al., *Energy Storage Mater.*, **43**, 391 (2021).
19. Z. Zhang et al., *Angew. Chemie*, **133**, 16540 (2021).
20. B. Ge et al., *Small*, **15**, 1902220 (2019).
21. Y. Hou et al., *Adv. Funct. Mater.*, **27**, 1700564 (2017).
22. C. Yang, K. Guo, D. Yuan, J. Cheng, and B. Wang, *J. Am. Chem. Soc.*, **142**, 6983 (2020).
23. J. Chen et al., *Adv. Mater.*, **31**, 1805484 (2019).
24. X. Li et al., *Adv. Mater.*, **31**, 1905879 (2019).
25. S. Li et al., *Energy Environ. Sci.*, **11**, 1318 (2018).
26. S. Thoka et al., *ACS Appl. Mater. Interfaces*, **12**, 17353 (2020).
27. Q. Deng et al., *Adv. Energy Mater.*, **12**, 2103667 (2022).
28. N. Acharya and R. Sagar, *Inorg. Chem. Commun.*, **132**, 108856 (2021).
29. K. L. Nardi, N. Yang, C. F. Dickens, A. L. Strickler, and S. F. Bent, *Adv. Energy Mater.*, **5**, 1500412 (2015).
30. P.-P. Liu, Y.-Q. Zheng, H.-L. Zhu, and T.-T. Li, *ACS Appl. Nano Mater.*, **2**, 744 (2019).
31. H. Liu et al., *J. Mater. Chem. A*, **10**, 4817 (2022).
32. P.-F. Zhang et al., *ACS Catal.*, **10**, 1640 (2020).
33. L. Liu et al., *ACS Appl. Mater. Interfaces*, **12**, 33846 (2020).
34. F. Jing et al., *Energy Storage Mater.*, **49**, 164 (2022).
35. J. Zhang, Y. Sun, X. Li, and J. Xu, *Sci. Rep.*, **9**, 18121 (2019).
36. L. Fan et al., *Adv. Mater.*, **34**, 2204134 (2022).
37. H. Sheng et al., *Adv. Mater.*, **34**, 2108947 (2022).
38. Y. Wang et al., *Adv. Funct. Mater.*, **32**, 2202737 (2022).
39. H. Huo et al., *Nano Energy*, **61**, 119 (2019).